









## RESEARCH ARTICLE

[View Article Online](#)  
[View Journal](#) | [View Issue](#)Cite this: *RSC Med. Chem.*, 2023, 14, 2035

# The rational design of ARUK2007145, a dual inhibitor of the $\alpha$ and $\gamma$ isoforms of the lipid kinase phosphatidylinositol 5-phosphate 4-kinase (PI5P4K) $\dagger$

Gregory G. Aldred,  $\ddagger$  Timothy P. C. Rooney,  $\ddagger$  Henriette M. G. Willems,   
Helen K. Boffey,  $\ddagger$  Christopher Green,  $\S$  David Winpenny, John Skidmore,   
Jonathan H. Clarke  and Stephen P. Andrews  $\star$ 

The phosphatidylinositol 5-phosphate 4-kinases (PI5P4Ks) are therapeutic targets for diseases such as cancer, neurodegeneration and immunological disorders as they are key components in regulating cell signalling pathways. In an effort to make probe molecules available for further exploring these targets, we have previously reported PI5P4K $\alpha$ -selective and PI5P4K $\gamma$ -selective ligands. Herein we report the rational design of PI5P4K $\alpha/\gamma$  dual inhibitors, using knowledge gained during the development of selective inhibitors for these proteins. ARUK2007145 (39) is disclosed as a potent, cell-active probe molecule with ADMET properties amenable to conducting experiments in cells.

Received 20th July 2023,  
Accepted 23rd August 2023

DOI: 10.1039/d3md00355h

[rsc.li/medchem](http://rsc.li/medchem)

## Introduction

Cellular phospholipids are structural components that delineate the outer boundary of the cell as well as all membrane-bound organelles and compartments. In addition to this structural role these lipids have also been shown to have various other functions, and the phosphoinositides, whilst a minor component of the total cellular phospholipid content, are prolific in their involvement in additional essential cellular processes such as membrane-trafficking, cell proliferation, cytoskeletal organisation, channel regulation and involvement in cell stress and death responses.<sup>1–4</sup> The canonical route for phosphoinositide signalling results in the production of inositol trisphosphate (InsP3) from phosphatidylinositol (4,5) bispophosphate (PI(4,5)P<sub>2</sub>) as a result of lipase activity, to facilitate cellular calcium release.<sup>5</sup> Subsequently each of the seven different phosphatidylinositol phosphate species (defined by the phosphorylation state (mono-, bis- or tris-) of positions 3–5 of the 6-carbon ring that

constitutes the hydrophilic phosphatidylinositol headgroup<sup>1</sup>) have also been shown to have specific cellular functions, which can be location and cell-type specific.<sup>1,6</sup> The interconversion of this phosphorylation state is controlled by a group of kinases and phosphatases that may act synergistically to remove or create localised pools of phosphoinositide that can directly (allosteric activation of proteins, regulation of membrane proteins such as ion channels) or indirectly (protein recruitment to membranes *via* specific phosphoinositide-binding or adapter proteins) result in downstream signalling events.<sup>1,2</sup>

Phosphatidylinositol 5-phosphate (PI5P) is converted to PI(4,5)P<sub>2</sub> by a family of phosphatidylinositol 5-phosphate 4-kinases (PI5P4Ks) consisting of three distinct isoforms; alpha, beta and gamma. Heterogeneity exists within the family; the alpha isoform, *in vitro*, is the most catalytically active,<sup>7</sup> whereas the gamma isoform has very low intrinsic activity.<sup>8</sup> The beta isoform is the only one to contain a recognised nuclear localisation sequence.<sup>9</sup> Although all isoforms are generally ubiquitously expressed, tissue specific differences have been observed.<sup>8</sup> Diverse cellular functions have also been associated with the different isoforms, for example PI5P4K $\beta$  and PI5P4K $\gamma$  may have roles as GTP sensors,<sup>10</sup> and both PI5P4K $\alpha$  and PI5P4K $\gamma$  have been shown to associate to autophagic structures.<sup>11,12</sup> Hence the different specific roles reported for each of the isoforms could be functions that are tissue or cell-type specific, or spatially or temporally differentiated in response to activation of different metabolic pathways. Structurally there

The ALBORADA Drug Discovery Institute, University of Cambridge, Island Research Building, Cambridge Biomedical Campus, Hills Road, Cambridge, CB2 0AH, UK.  
E-mail: [spa26@cam.ac.uk](mailto:spa26@cam.ac.uk)

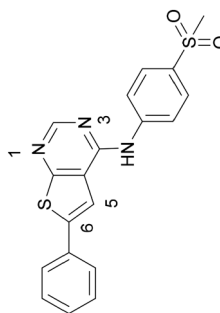
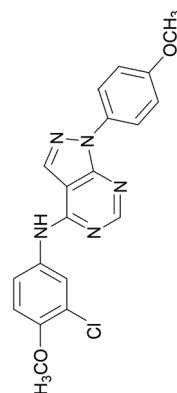
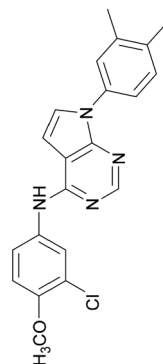
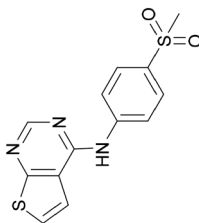
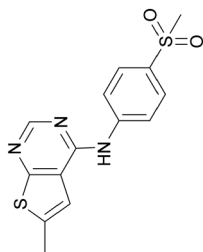
$\dagger$  Electronic supplementary information (ESI) available. See DOI: <https://doi.org/10.1039/d3md00355h>

$\ddagger$  These authors contributed equally.

$\S$  Present address: UK Dementia Research Institute, University of Cambridge, Island Research Building, Cambridge Biomedical Campus, Hills Road, Cambridge, CB2 0AH, UK.

Table 1 Previously reported PI5P4K ligands 1–5

Compound	Inhibition of PI5P4K			Physicochemical properties	
	PI5P4K $\alpha$ pIC <sub>50</sub>	PI5P4K $\gamma$ + pIC <sub>50</sub>	Fold-selectivity ( $\alpha$ IC <sub>50</sub> / $\gamma$ IC <sub>50</sub> )	M <sub>w</sub>	XlogP
1	<4.8	7.1	>210	319	2.8
2	<4.3	6.5	>170	305	2.6
3	8.0	<4.3	<0.0002	379	5.8
4	6.4	4.9	0.032	382	4.2
5	<5.3	7.4	>130	381	4.5



are also differences between the isoforms<sup>9,13</sup> but it is clear that each is able to heterodimerise,<sup>7,8</sup> which leads to the intriguing possibility that isoforms are able to regulate the localisation, specific function or *in vivo* activity of each other.

The promiscuity of the phosphoinositides in cellular signalling pathways has implications for disease as enzyme dysfunction or misregulation may be causative in various developmental disorders, inflammation and infection.<sup>13–16</sup> As oncology targets, PI5P4Ks have become increasingly associated with a number of diseases.<sup>17</sup> Interestingly the involvement of PI5P4K $\alpha$  alone has been documented in glioblastoma, acute myeloid leukemia (AML) and prostate cancer<sup>18–21</sup> but other examples suggest that there may be a combinatorial role for the PI5P4Ks. Both PI5P4K $\alpha$  and PI5P4K $\beta$  are involved in p53-deficient breast cancer and soft tissue sarcomas<sup>22,23</sup> and high expression of both PI5P4K $\alpha$  and PI5P4K $\gamma$  associate with unfavourable clinical outcome in AML.<sup>24</sup>

Several recent reports detail inhibitors for PI5P4Ks, not only pan-specific<sup>25–29</sup> but also isoform specific.<sup>30–34</sup> Emerging tools are also being developed for dual-specific inhibitors for PI5P4K $\alpha$  and PI5P4K $\beta$ <sup>22,35</sup> and methods have also been reported for removing protein completely in cells using PROTAC systems, such as JWZ-1-80 for PI5P4K $\gamma$ ,<sup>36</sup> which will be useful to interrogate non-catalytic roles. Here we present a new tool that can be used to investigate the impact of dual inhibition of both the PI5P4K $\alpha$  and PI5P4K $\gamma$  isoforms.

We have previously reported PI5P4K $\gamma$ -selective inhibitors including ARUK2001607 (**1**) which was derived from virtual screening hit **2**,<sup>30</sup> as well as PI5P4K $\alpha$ -selective inhibitors including tool compound ARUK2002821 (**3**) which was derived from virtual screening hit **4** (ref. 33) (Table 1). During the course of those studies, we also became interested in developing dual PI5P4K $\alpha$ –PI5P4K $\gamma$  inhibitors as probe molecules. In particular, we had observed small amounts of PI5P4K $\alpha$  inhibition in some analogues of **1** which we were able to further optimise through rational design. Herein we describe efforts to further increase the level of PI5P4K $\alpha$  activity in the **1** chemotype towards the development PI5P4K $\alpha$ / $\gamma$  dual inhibitors with IC<sub>50</sub> fold-selectivities within approximately 10-fold in either direction.

## Results

Compound **5** was a lead in the development of our novel dual PI5P4K inhibitors. Compared to **1** and many of the other analogues previously explored in this chemical series,<sup>30,37</sup> **5** was differentiated by having a larger substituent at the 6-position of the thienylpyrimidine core (Table 1). This group gave a point of diversity for further SAR exploration and this compound appeared to be on the threshold of detection in the PI5P4K $\alpha$  ADP-Glo assay, sometimes giving a partial inhibition curve leading to an

inconsistent pIC<sub>50</sub> with hints that the vector at the 6-position of the thienylpyrimidine core may be of value introducing further PI5P4K $\alpha$  activity.

As the phenyl group of **5** had an increased  $M_w$  and Xlog  $P$  compared to **1** we also focussed on improving physicochemical properties during iterations of compound design. In particular, we were keen to introduce heteroatoms in this ring to modulate Xlog  $P$ . The first synthesised compound of this type, **6**, shows a marked decrease in Xlog  $P$  compared to **5** and was found to have increased potency for PI5P4K $\alpha$  and PI5P4K $\gamma$ + (Table 2).<sup>37</sup> When the 8BQ4 crystal structure of PI5P4K $\gamma$  was later solved with **1** bound in the ATP binding site, docking of **6** suggested that its pyridyl N might interact with Lys216 of PI5P4K $\gamma$  (Fig. 1).

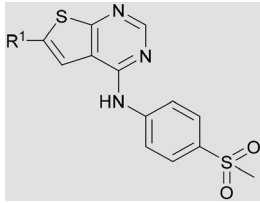
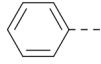
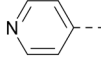
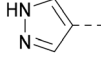
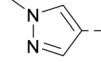
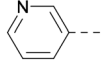
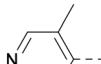
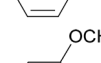
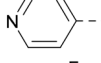
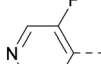
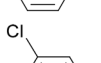
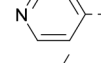
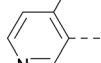
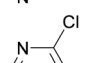
Indeed, a range of heterocycles was tolerated at the 6-position of the thienylpyrimidine, with PI5P4K $\gamma$ + activity being retained when compared to **5** and many showed some level of PI5P4K $\alpha$  inhibition as well as a reduction in Xlog  $P$  (Table 2). Pyrazoles **7** and **8** retained good levels of PI5P4K $\gamma$ + inhibition whilst showing some PI5P4K $\alpha$  inhibition (Table 2). Pyridine **9** showed higher selectivity towards PI5P4K $\gamma$ + than **6** (160 vs. 63-fold, respectively). The relative PI5P4K $\alpha$  activity of **6** could be increased by methylation of the pyridyl 3-position (**10**) more effectively than by addition of OMe (**11**), or F (**12**) at the same position, or by chlorination at the pyridyl 2-position (**13**; Table 2). A range of small substituents was also trialled on template **6** and these were generally well tolerated (see **14–17**). Compound **17** was a useful lead from this set with a good balance of activity at PI5P4K $\alpha$  and  $\gamma$ + as well as one of the lower Xlog  $P$ s in this series. Compound **17** was therefore selected as a template for further exploration around the sulfone group.

Fig. 1 shows that the arylsulfone of dual inhibitor **6** is predicted to overlay well with the corresponding group of the PI5P4K $\gamma$ -selective molecule **1** in the PI5P4K $\gamma$  structure (8BQ4). A question remained as to whether the corresponding group of PI5P4K $\alpha$ -selective **3** (*i.e.* 3,4-dimethylphenyl) would transpose onto this thienylpyrimidine template (Fig. 2). Using **17** as the optimal compound from Table 2, the dimethylphenyl group of **3** was transposed to provide compound **18**, which was docked into the **3** structure (8C8C, Fig. 2).

The rationally-designed compound **18** was found to have improved PI5P4K $\alpha$  activity compared to **17** but diminished PI5P4K $\gamma$ + activity (Table 3). An alternative potent PI5P4K $\alpha$  inhibitor with a 2,4-dimethylphenyl group, “compound **25**”,<sup>33</sup> was also merged onto the thienylpyrimidine core to give the resulting compound **19**. Both **18** and **19** are dual PI5P4K $\alpha$ / $\gamma$ + inhibitors, as predicted. Indeed, the designed modifications increased the PI5P4K $\alpha$  activity of this chemotype to the point that, relative to PI5P4K $\gamma$ -selective starting point **1**, both **18** and **19** showed higher levels of PI5P4K $\alpha$  than PI5P4K $\gamma$ + inhibition (for reference, compound **1** showed no detectable inhibition of PI5P4K $\alpha$  under the same assay conditions, Table 1).



Table 2 Variation of  $R^1$  to introduce heteroaryl groups

		Inhibition of PI5P4K			Physicochemical properties	
		PI5P4K $\alpha$ pIC <sub>50</sub>	PI5P4K $\gamma$ + pIC <sub>50</sub>	Fold-selectivity ( $\alpha$ IC <sub>50</sub> / $\gamma$ IC <sub>50</sub> )	$M_W$	$X \log P$
5		<5.3	7.4	>130	381	4.5
6		5.9	7.7	63	382	3.1
7		5.9	7.8	79	371	3.7
8		5.2	7.4	160	385	3.1
9		5.3	7.5	130	382	3.1
10		6.2	7.9	50	396	3.4
11		5.6 <sup>a</sup>	7.5 <sup>a</sup>	79	412	3.1
12		<4.6	7.0	>250	400	3.2
13		5.1 <sup>a</sup>	7.2	130	417	4.2
14		6.0	7.9	79	396	3.4
15		6.2	7.9	50	417	4.2
16		5.8 <sup>a</sup>	7.5	50	400	3.7
17		6.0	7.7	50	396	3.3

<sup>a</sup> Inconsistent pIC<sub>50</sub> measurements between replicates; value shown is upper limit.

Lipophilic substituents at  $R^2$  have previously been found to be important for PI5P4K $\alpha$  inhibition.<sup>33</sup> As such, a variety of other lipophilic groups was tested at this position (Table 3). Compounds **20** and **21** were modest dual inhibitors and an interesting SAR trend was observed for the series of small aliphatic groups for **22–24**, which increased in both PI5P4K $\alpha$  and PI5P4K $\gamma$ +

activity with increasing size of the *para* substituent. In agreement with the hypothesis that the polar sulfone of **17** was not favourable for PI5P4K $\alpha$  inhibition, apolar sulphide **25** was synthesised. This molecule showed an expected increase in PI5P4K $\alpha$  inhibition with a modest reduction in PI5P4K $\gamma$ + inhibition to afford a potent dual inhibitor.



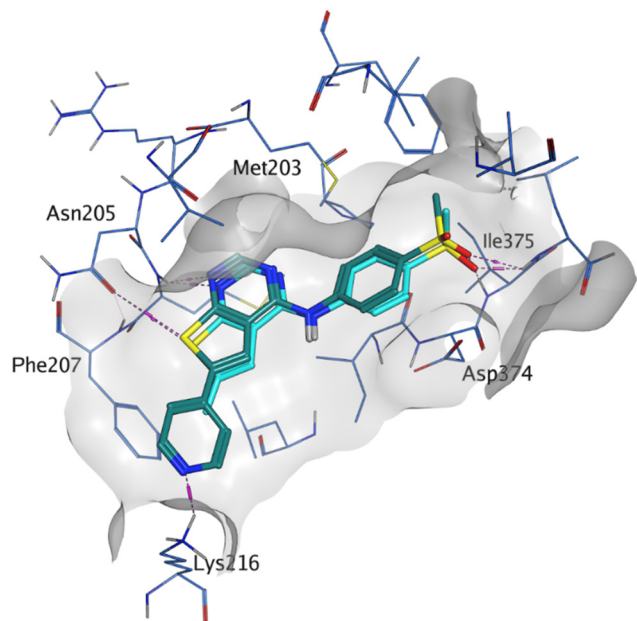


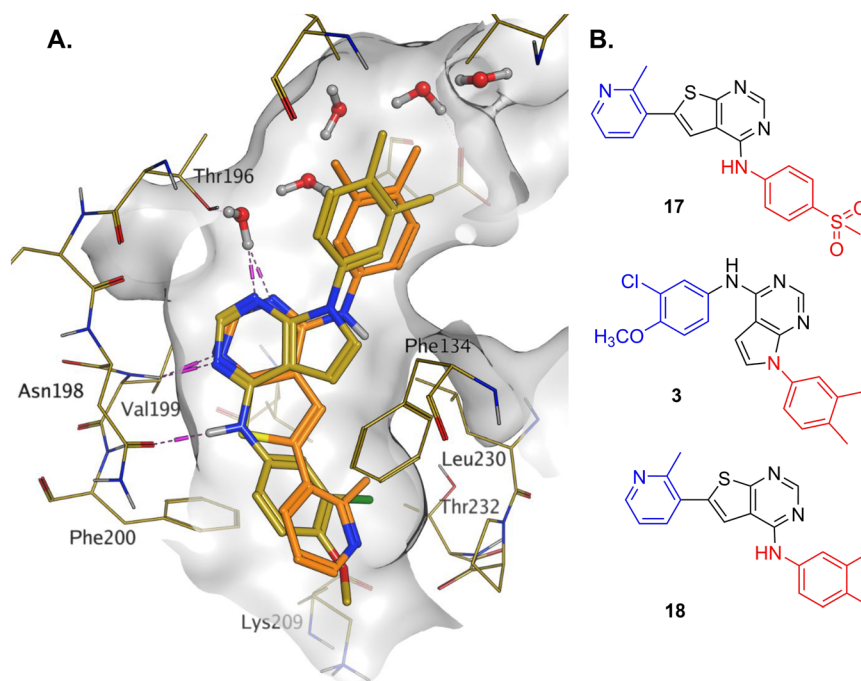
**Fig. 1** Compound **6** (green) docked into the 8BQ4 structure of PI5P4K $\gamma$ -1 (cyan).

Following on from this, combinations of groups which had been productive at  $R^1$  and  $R^2$  were explored (Table 4). Owing to the preference for lipophilic groups at  $R^2$ , it was desirable to use polar heterocyclic groups at position  $R^1$ , where possible, to help offset  $X\log P$ . Nonetheless, these compounds were generally high in  $X\log P$ , typically in the range 4–5 (compounds 26–30).

Substitution at the 5-position of the thienopyrimidine core was also investigated (Table 5). In general, this position was tolerant of a wide range of substituents from small lipophilic groups such as methyl (**31**) and chloro (**32**), to larger substituents such as a small ring (**33**) or a much larger group incorporating a polar amide moiety (**34**). A 5,6-disubstituted thiophene was also tolerated (**35**). However, these derivatives did not offer an advantage over 6-substituted thienylpyrimidines and were not pursued further.

The thiophene was also ‘reversed’ from thieno[2,3-*d*]pyrimidines to afford thieno[3,2-*d*]pyrimidine derivatives such as **36**, which is a direct analogue of **2** but with the sulfur atom moved within the thiophene ring (Table 6). Compound **36** shows a higher PI5P4K $\gamma$   $pIC_{50}$  than **2** (7.3 vs. 6.5, respectively) and both compounds had undetectable levels of PI5P4K $\alpha$  inhibition. Matched pairs of molecules in which the regiochemistry of the thienopyrimidine was alternated while the R groups were kept constant showed that thieno[3,2-*d*]pyrimidine was generally the more active regioisomer. For example, compound **38** forms a matched pair with **24** with the former being slightly more active at both isoforms (PI5P4K $\alpha$  7.0 vs. 6.6, respectively, and PI5P4K $\gamma$  7.3 vs. 7.0). Similarly, **39** forms a matched pair with **28**, with **39** being slightly more active at both PI5P4K isoforms. The thieno[3,2-*d*]pyrimidine template was also used to explore further alternative lipophilic groups at  $R^2$  (**40**, **41**) and a group from potent PI5P4K $\gamma$  inhibitor ‘compound 7’ (**42**).<sup>30</sup>

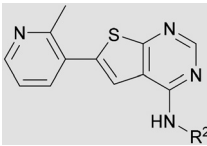
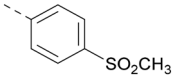
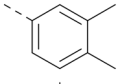
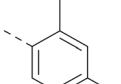
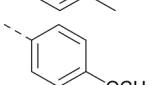
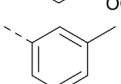
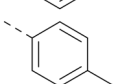
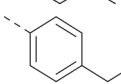
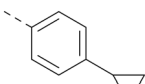
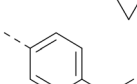
A selection of the more active compounds identified to this point was profiled for PI5P4K $\beta$  activity as well as PI5P4K $\gamma$



**Fig. 2** A) Compound **18** (orange) docked into the 8C8C structure of PI5P4K $\alpha$ -3 (gold). The dimethylphenyl group of **3** overlays well with that of **18**; B) 2D comparison of **3**, **17** and **18**.



Table 3 Exploration of  $R^2$ 

		Inhibition of PI5P4K			Physicochemical properties	
		PI5P4K $\alpha$ pIC <sub>50</sub>	PI5P4K $\gamma$ + pIC <sub>50</sub>	Fold-selectivity ( $\alpha$ IC <sub>50</sub> / $\gamma$ IC <sub>50</sub> )	$M_w$	$X \log P$
17		6.0	7.7	50	396	3.3
18		6.5	5.9	0.25	346	4.7
19		5.5	5.4	0.79	346	4.7
20		5.9	5.7	0.69	348	4.1
21		5.5	5.3	0.63	332	4.4
22		6.2	5.8	0.4	332	4.4
23		6.2	6.4	1.6	346	4.8
24		6.6	7.0	2.5	358	4.9
25		6.6	7.3	5.0	364	4.8

WT activity and cell penetration in a PI5P4K-WT InCELL Pulse cellular target engagement assay (Table 7). Both assays have previously been described for screening PI5P4K $\gamma$  inhibitors.<sup>38</sup> All compounds tested in the PI5P4K $\beta$  ADP-Glo assay returned IC<sub>50</sub>s > 10  $\mu$ M (Table 7). Furthermore, there is a good correlation between the pIC<sub>50</sub>s obtained in the PI5P4K $\gamma$ + ADP-Glo assay and the PI5P4K-WT InCELL Pulse assay, confirming that these compounds are *bona fide* inhibitors of the wild-type form of PI5P4K $\gamma$ . In general, there is a slight drop in pIC<sub>50</sub> in the cellular assay, possibly owing to the requirement for cell permeability and/or the non-specific binding of the compounds to cellular components; however, these compounds such as **10** and **39** are potent PI5P4K $\gamma$  inhibitors in live cells.

Compounds with interesting profiles were selected for screening in further assays to assess ADMET properties with the aim of identifying potent dual inhibitors that would make suitable probes for applications in cellular experiments (Table 8). As such, cell permeability and efflux were measured in MDCK-MDR1 cells and aqueous solubility was measured at pH 7.4. To give an indication as to whether any of these probes may be suitable for *in vivo* testing, stability in mouse

liver microsomes (MLMs) was also measured. In general, there was a wide range of values in each of the ADMET assays for this series of molecules. Efflux ratios varied from good (0.91) to very high (64). Cell permeabilities were generally good, ranging from low at  $1.3 \times 10^{-6}$  cm s<sup>-1</sup> to high at  $14.2 \times 10^{-6}$  cm s<sup>-1</sup>. Solubilities ranged from low to moderate (1–30  $\mu$ M). Half-lives in MLMs ranged from very poor to very good (0.94–383 minutes).

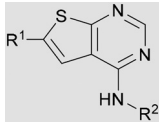
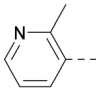
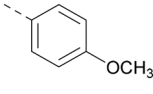
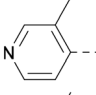
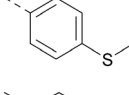
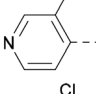
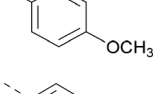
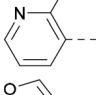
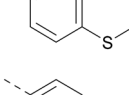
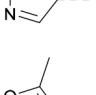
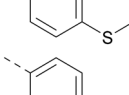
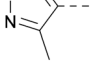
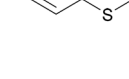
Compound **39** showed one of the most balanced profiles required for a cell-active probe: good permeability, no efflux and moderate solubility. This molecule shows good activity in the InCELL Pulse target engagement assay (PI5P4K $\gamma$  pIC<sub>50</sub> = 7.3) and a good dual activity in the ADP-Glo assays showing similar activities for PI5P4K $\gamma$ + and PI5P4K $\alpha$  (fold-selectivity = 5). However, **39** has a very high turnover in MLMs and is unlikely to make a useful *in vivo* tool (MLM  $t^{1/2}$  = 0.44 min). Compound **39** (ARUK2007145) is therefore nominated as a PI5P4K $\alpha/\gamma$  dual inhibitor probe molecule for cell experiments.

Other compounds of note are **32**, which shows good ADMET properties in general, but is slightly less active than **39**, particularly at PI5P4K $\alpha$ , and the cluster of compounds **8**,

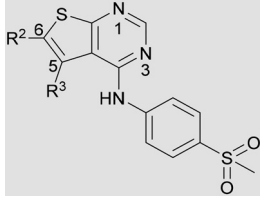
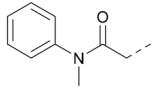




**Table 4** Combinations of  $R^1$  and  $R^2$  groups which, individually, had given advantages in Tables 2 and 3

			Inhibition of PI5P4K			Physicochemical properties	
	$R^1$	$R^2$	PI5P4K $\alpha$ pIC <sub>50</sub>	PI5P4K $\gamma$ + pIC <sub>50</sub>	Fold-selectivity ( $\alpha$ IC <sub>50</sub> / $\gamma$ IC <sub>50</sub> )	$M_W$	$X \log P$
20			5.9	5.7	0.69	348	4.1
26			6.9	7.7	6.9	364	4.8
27			6.2	6.2	1.1	348	4.2
28			6.6	7.7	12	385	5.6
29			6.6	7.4	6.0	340	4.0
30			6.8	7.6	6.3	368	4.4

**Table 5** 5-Substituted thieno[2,3-d]pyrimidine analogues

			Inhibition of PI5P4K			Physicochemical properties	
	$R^2$	$R^3$	PI5P4K $\alpha$ pIC <sub>50</sub>	PI5P4K $\gamma$ + pIC <sub>50</sub>	Fold-selectivity ( $\alpha$ IC <sub>50</sub> / $\gamma$ IC <sub>50</sub> )	$M_W$	$X \log P$
9	3-Pyridyl	H	5.3	7.5	130	382	3.1
31	H	CH <sub>3</sub>	<4.3	7.3	>980	319	2.9
32	H	Cl	<6.2	7.3	11	340	3.2
33	H	<i>c</i> -Pr	<4.8	7.0	140	345	3.4
34	H		5.6	7.3	50	439	4.2
35	CH <sub>3</sub>	CH <sub>3</sub>	<4.3	6.7	>250	333	3.1

15 and 37, which fall into the category of having a high MLM half-life and good PI5P4K $\gamma$  activity, but lower PI5P4K $\alpha$  activity. All of these compounds have a 4-(methylsulfonyl) phenyl group at position  $R^2$ . The polar methyl sulfonyl group is detrimental for PI5P4K $\alpha$  activity but positively modulates microsomal stability, whereas more lipophilic groups in place of the methylsulfonyl group positively modulate PI5P4K $\alpha$  activity but are metabolically liable. Nonetheless, compounds

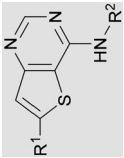
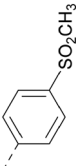
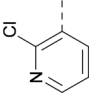
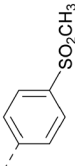
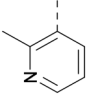
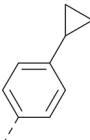
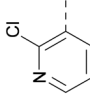
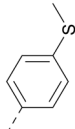
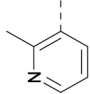
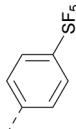
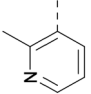
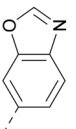
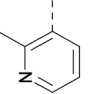
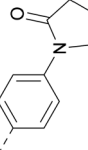
8, 15 and 37, all have higher PI5P4K $\alpha$  activities than previously reported compounds from this class<sup>30</sup> and may make useful complementary probes.

## Discussion

Rational design of dual PI5P4K $\alpha$ –PI5P4K $\gamma$  inhibitors such as 39 began with the observation that 5 offers a new vector for



Table 6 Thieno[3,2-d]pyrimidine analogues

			Inhibition of PI5P4K			Physicochemical properties	
	R <sup>1</sup>	R <sup>2</sup>	PI5P4K $\alpha$ pIC <sub>50</sub>	PI5P4K $\gamma$ + pIC <sub>50</sub>	Fold-selectivity ( $\alpha$ IC <sub>50</sub> / $\gamma$ IC <sub>50</sub> )	M <sub>w</sub>	XlogP
36	H -		<4.3	7.3	1000	305	2.6
37			6.5	7.9	5.4	417	4.2
38			7.0	7.3	1.9	358	4.9
ARUK2007145 (39)			7.3	8.1	5	385	5.6
40			6.2	7.0	6.3	444	6.2
41			5.5	6.3	5.9	359	4.6
42			7.0	8.1	13	401	4.4





**Table 7** PI5P4K $\alpha$ ,  $\beta$  and  $\gamma$  inhibition (ADP-Glo) and PI5P4K $\gamma$  cellular target engagement (InCELL Pulse) for selected compounds

	ADP-Glo pIC <sub>50</sub>			InCELL Pulse pIC <sub>50</sub>
	PI5P4K $\alpha$	PI5P4K $\beta$	PI5P4K $\gamma$ +	PI5P4K $\gamma$ -WT
5	<5.3	<4.6	7.4	6.6
8	5.2	4.9	7.4	6.7
10	6.2	4.9	7.9	7.7
15	6.2	4.9	7.9	7.1
17	6.0	4.7	7.7	7.3
37	6.5	ND	7.9	7.4
39	7.3	ND	8.1	7.3

SAR exploration. Using the novel vector provided by the aryl ring at position 6 of 5's core, further iterations of design led to PI5P4K $\alpha$ -active compounds with improved physicochemical properties over 5, particularly  $X\log P$

(Table 2). For example, **14** is a more polar derivative which docked well in the PI5P4K $\gamma$  structure, 8BQ4 (Fig. 3A). However, not all compounds docked well in this orientation, *e.g.* **30** shows different docking pose in 8BQ4 (Fig. 3B). The thioether of **30** appears to prefer a conformation where the aniline has rotated 180 degrees from the 8BQ4 orientation (Fig. 3B), so that the NH is pointing outwards. Thus, it is possible that the nature of the substituent on the aniline may influence the conformational preference at the  $\psi$  dihedral angle, and therefore also impact on the predicted binding pose.

Later in the program, liganded PI5P4K $\alpha$  crystal structures became available which allowed further structural assessment. The 8C8C PI5P4K $\alpha$  structure shows ligand **3** in a binding mode in which, compared to **1** in the 8BQ4 PI5P4K $\gamma$  structure, has the aminopyrimidine flipped so that N2 rather than N4 is making an

**Table 8** ADMET data for selected compounds

	Efflux ratio <sup>a</sup>	$P_{app}$ <sup>a</sup> (A2B, 10 <sup>-6</sup> cm s <sup>-1</sup> )	Solubility <sup>b</sup> ( $\mu$ M)	MLM $t_{1/2}$ <sup>c</sup> (min)
5	1.3	6.23	1	54.5
8	26.4	2.88	30	73.3
10	25.2	3.13	30	9.23
14	34.1	2.45	30	8.2
15	15.7	4.73	3	383
17	64.3	1.33	10	35.5
26	1.1 <sup>d</sup>	3.7 <sup>d</sup>	3	0.94
32	3.7	14.2	10	51.4
37	31.8	1.33	10	70.8
38	0.91	9.95	3	1.94
39	0.98	12.9	10	0.44
42	27.4	3.15	10	5.39

<sup>a</sup> Permeability and efflux ratios determined in MDCK-MDR1 cells. <sup>b</sup> Aqueous solubility at pH 7.4. <sup>c</sup> Mouse liver microsome stability (half-life).

<sup>d</sup> Recovery low A2B; possible solubility or binding issues; accuracy of result questionable.

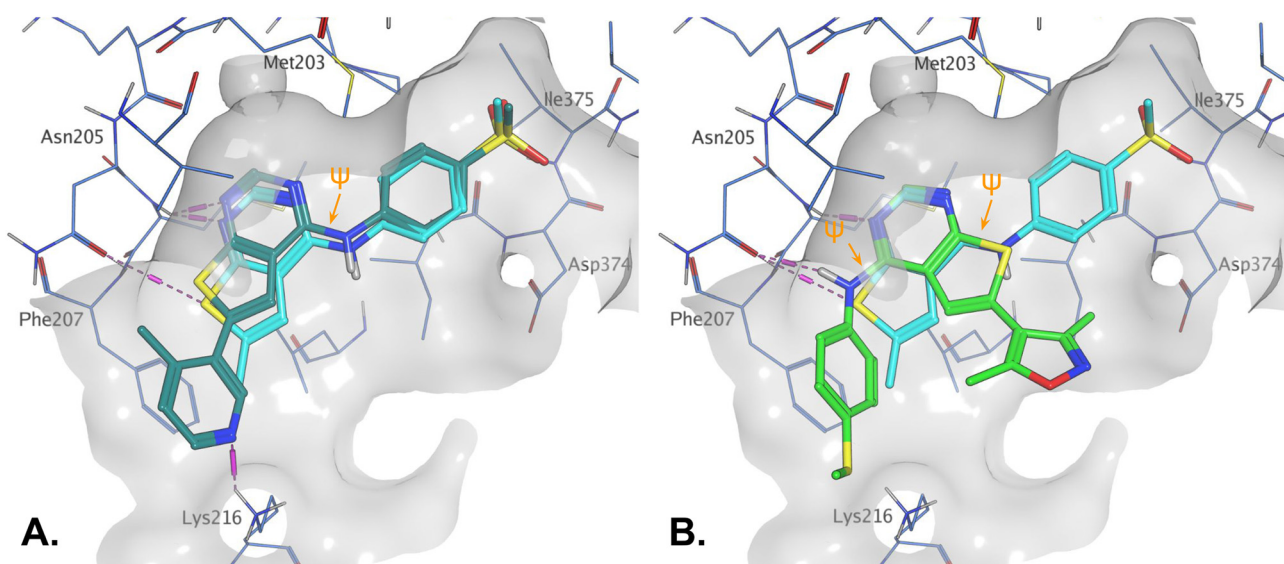


**Fig. 3** A) Compound **14** (teal); B) compound **30** (green) docked to PI5P4K $\gamma$  structure (8BQ4). Compound **1** shown for reference in both (cyan). The  $\psi$  dihedral angle is indicated in orange, this changes from 4° for **1** and **14** to 170° for **30**.



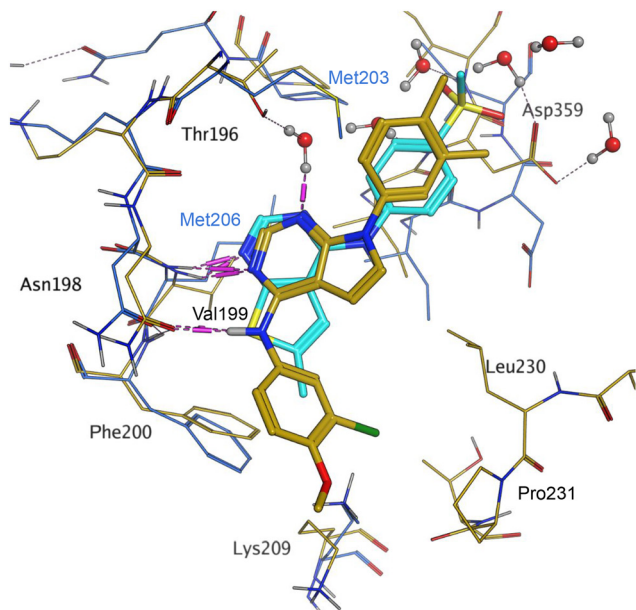


**Fig. 4** Compound **3** and PI5P4K $\alpha$  protein (pdb 8C8C; gold) superimposed onto **1** and PI5P4K $\gamma$  protein (pdb 8BQ4; cyan), aligned using the hinge residues Thr196–Phe200 (numbering from PI5P4K $\alpha$  sequence). This shows that the pyrimidine moiety does not bind in the same orientation in the PI5P4K $\alpha$  and PI5P4K $\gamma$  ligands. PI5P4K $\alpha$  residues are labelled in black and PI5P4K $\gamma$  residues in blue.

interaction with the hinge (Val199NH in PI5P4K $\alpha$ , Met206 in PI5P4K $\gamma$ ; Fig. 4). In the PI5P4K $\alpha$  structure (8C8C) the aniline NH of **3** is also interacting with the hinge (Asn98OD1), whereas in the PI5P4K $\gamma$  structure (8BQ4) the aniline NH of **1** is not near the hinge residues. Retrospective docking suggested that our dual PI5P4K $\alpha$ /PI5P4K $\gamma$  ligands **14** and **18** can interact with PI5P4K $\alpha$  in two different poses, one is 1-like (Fig. 5A) and the other 3-like (Fig. 5B). For most of the dual inhibitors discussed here, the binding mode for **14** (shown in Fig. 5B) is only

accessible in a protein conformation where Leu230 and Pro231 are not near the active site (seen, for example, in the PI5P4K $\alpha$  structure solved with BAY297 bound, pdb 6YM4),<sup>31</sup> as these two residues clash with the  $R^1$  extension in the 8C8C protein structure. Docking favours the pose shown in Fig. 5B for thieno[2,3-*d*] pyrimidines with an  $R^1$  3-pyridine and an acceptor atom in  $R^2$ , e.g. **9**, **14**, **15**, **16** and **17**. This appears to be driven by interactions with Lys145 and Lys209. In contrast, the thieno[3,2-*d*]pyrimidines (Table 6) all adopt the pose shown in Fig. 5A in preference. This may stem from a lower conformational energy for the extended conformation shown in Fig. 5A for this core, or perhaps the thiophene C–H offers a better interaction with the side chain of Asn198 than the sulphur.

Interestingly, all of the ligands with good PI5P4K $\alpha$  activities ( $\text{pIC}_{50} > 6.5$ ), with the exception of **42**, have a much better docking score in the PI5P4K $\alpha$ –3 structure (8C8C) than the PI5P4K $\alpha$ –BAY297 (6YM4) structure (see ESI† Table S1).

## Conclusions

The phosphatidylinositol 5-phosphate 4-kinases (PI5P4Ks) play a central role in regulating cell signalling pathways and, as such, have become therapeutic targets for diseases such as cancer, neurodegeneration and immunological disorders but useful probe molecules have only recently become available to further study these systems. To expand the tools available to the field, herein we disclose compound **39** and a series of related PI5P4K $\alpha$ / $\gamma$  dual inhibitors which were developed from a PI5P4K $\gamma$ -selective series, using rational approaches starting from PI5P4K $\alpha$ -selective ligands and PI5P4K $\gamma$ -selective ligands. We anticipate that these tools will enable further discoveries in the field.

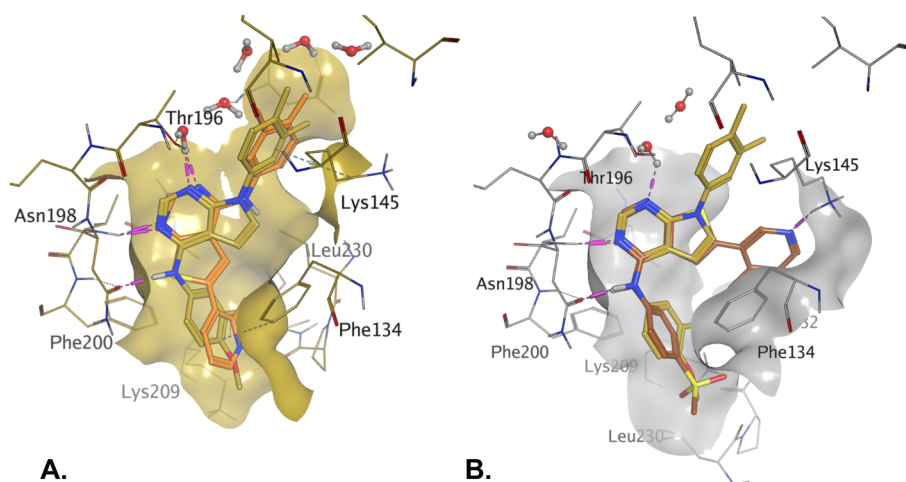


**Fig. 5** A) The dimethylphenyl group of **3** bound to PI5P4K $\alpha$  (pdb 8C8C; gold) overlays well with that of **18** (orange) as positioned by docking to the 8C8C structure; B) **14** (brown) docked to alternative PI5P4K $\alpha$  structure pdb 6YM4 (grey); **3** (pdb 8C8C; gold) was transposed onto the 6YM4 structure by alignment.



## Experimental details

### Biochemical assays

Assays to determine kinase activity of PI5P4K $\alpha$  and PI5P4K $\gamma$  in the presence of inhibitors using an ADP-Glo assay (Promega) were performed as described previously.<sup>38</sup> Recombinant PI5P4K protein was prepared as described previously.<sup>8</sup> *E. coli* BL21(DE3) clones harbouring PI5P4K $\alpha$  (PIP4K2A; UniGene 138363), PI5P4K $\beta$  (PIP4K2B; UniGene 171988) or PI5P4K $\gamma$  (PIP4K2C; UniGene 6280511), cloned into pGEX6P plasmid (Cytiva), were used to overexpress these proteins. PI5P4K $\gamma$  protein (designated “PI5P4K $\gamma$ +”) was a genetically modified chimera of PI5P4K $\gamma$  with a specific activity close to that of the active PI5P4K $\alpha$  isoform<sup>8</sup> and carries a number of PI5P4K $\alpha$ -like mutations; insertion of three amino acids (QAR) at 139 plus an additional 11 amino acid mutations: S132L, E133P, S134N, E135D, G136S, D141G, G142A, E156T, N198G, E199G and D200E. Cultures were induced with 0.4 mM IPTG overnight and probe-sonicated in the presence of protease inhibitors. GST fusion protein was harvested using a GSTrap FF affinity column (Cytiva) and the GST tag removed *in situ* with 50 U of PreScission protease (Cytiva) for 4 h at 4 °C. The cleaved protein was further purified by size-exclusion chromatography (ÅKTA Pure, Cytiva). The protein purity was confirmed by sodium dodecyl sulfate–polyacrylamide gel electrophoresis, and the concentration was determined by colorimetric assay (Bio-Rad).

Binding of compounds to PI5P4K $\gamma$  in intact cells was assessed using an InCELL Pulse thermal stabilisation assay (DiscoverX) as described previously.<sup>38</sup> PI5P4K $\gamma$  was cloned into the pICP vector (DiscoverX) to allow overexpression of the ePL-tagged target. Hek293 cells stably expressing ePL-tagged PI5P4K $\gamma$  were incubated with 25 nL of test compound in 100% DMSO in a black skirted PCR plate for 60 minutes at 38 °C. After incubation for 3 minutes at 46 °C, followed by cooling for 3 minutes at room temperature, 12  $\mu$ L of EA-3 reagent (prepared as per the manufactures guidelines) was added to each well. The plate was then incubated for 60 minutes in the dark prior to luminescence reading on a Pherastar FSX plate reader (BMG Labtech).

### Data analysis

Statistical analysis was performed using nonparametric testing in Prism 8 (GraphPad). Activity pIC<sub>50</sub> values and *in vivo* binding pEC<sub>50</sub> values were estimated using a 4-parameter fit (Dotmatics).

### Computational modelling

The virtual screening procedure was performed as previously described.<sup>30</sup> Dockings were performed using Glide SP (release 2022-3, Schrodinger, <https://www.schrodinger.com>). No constraints were used for docking. For 6YM4 docking the Lys209 conformation was changed to the rotamer that created the largest binding pocket using the MOE protein builder (release 22.02, Chemical Computing Group, <https://www.chemcomp.com>). Water molecules that are located in similar positions in 6YM4 and 8C8C were left in the site

during docking. The structures shown in Fig. 1 and 3 resulted from minimization of the binding site residues after docking to allow H-bonds with lysines to form.

## Abbreviations

ADME	Absorption, distribution, metabolism, excretion and toxicity
ATP	Adenosine triphosphate
GTP	Guanosine triphosphate
MDCK-MDR1	Madin Darby canine kidney-multidrug resistance mutation 1
MLM	Mouse liver microsomes
$M_w$	Molecular weight
ND	Not determined
$P_{app}$	Apparent permeability coefficient
PI5P4K	Phosphatidylinositol 5-phosphate 4-kinase
QM	Quantum mechanics
SAR	Structure–activity relationship
WT	Wild-type
$X \log P$	Log partition coefficient

## Author contributions

The manuscript was written through contributions of all authors. All authors have given approval to the final version of the manuscript. Stephen Andrews and Jonathan Clarke were programme leaders, John Skidmore offered further project leadership; together all three designed the project plan. Gregory Aldred, Timothy Rooney and Helen Boffey designed and synthesised the compounds. Henriëtte Willems performed computational chemistry and docked compounds. David Winpenny and Christopher Green ran ADP-Glo and InCELL Pulse assays and screened the compounds.

## Conflicts of interest

There are no conflicts of interest to declare.

## Acknowledgements

This work was funded by Alzheimer's Research UK (grant: ARUK-2015DDI-CAM), with support from the ALBORADA Trust. The ALBORADA Drug Discovery Institute is core funded by Alzheimer's Research UK (registered charity No. 1077089 and SC042474). The authors wish to thank Professor David C. Rubinsztein for insightful discussions on the PI5P4K biology.

## References

- 1 T. Balla, *Physiol. Rev.*, 2013, **93**, 1019–1137.
- 2 G. R. V. Hammond and J. E. Burke, *Curr. Opin. Cell Biol.*, 2020, **63**, 57–67.
- 3 Y. Posor, W. Jang and V. Haucke, *Nat. Rev. Mol. Cell Biol.*, 2022, **23**, 797–816.
- 4 M. C. Vidalle, B. Sheth, A. Fazio, M. V. Marvi, S. Leto, F.-D. Koufi, I. Neri, I. Casalin, G. Ramazzotti, M. Y. Follo, S. Ratti,





- L. Manzoli, S. Gehlot, N. Divecha and R. Fiume, *Biomolecules*, 2023, **13**, 1049.
- 5 M. J. Berridge and R. F. Irvine, *Nature*, 1989, **341**, 197–205.
  - 6 G. Di Paolo and P. De Camilli, *Nature*, 2006, **443**, 651–657.
  - 7 Y. Bultsma, W. J. Keune and N. Divecha, *Biochem. J.*, 2010, **430**, 223–235.
  - 8 J. H. Clarke and R. F. Irvine, *Biochem. J.*, 2013, **454**, 49–57.
  - 9 V. D. Rao, S. Misra, I. V. Boronenkov, R. A. Anderson and J. H. Hurley, *Cell*, 1998, **94**, 829–839.
  - 10 K. Sumita, Y.-H. Lo, K. Takeuchi, M. Senda, S. Kofuji, Y. Ikeda, J. Terakawa, M. Sasaki, H. Yoshino, N. Majd, Y. Zheng, E. R. Kahoud, T. Yokota, B. M. Emerling, J. M. Asara, T. Ishida, J. W. Locasale, T. Daikoku, D. Anastasiou, T. Senda and A. T. Sasaki, *Mol. Cell*, 2016, **61**, 187–198.
  - 11 M. R. Lundquist, M. D. Goncalves, R. M. Loughran, E. Possik, T. Vijayaraghavan, A. Yang, C. Pauli, A. Ravi, A. Verma, Z. Yang, J. L. Johnson, J. C. Y. Wong, Y. Ma, K. S. K. Hwang, D. Weinkove, N. Divecha, J. M. Asara, O. Elemento, M. A. Rubin, A. C. Kimmelman, A. Pause, L. C. Cantley and B. M. Emerling, *Mol. Cell*, 2018, **70**, 531–544.e9.
  - 12 M. Vicinanza, V. I. Korolchuk, A. Ashkenazi, C. Puri, F. M. Menzies, J. H. Clarke and D. C. Rubinshtein, *Mol. Cell*, 2015, **57**, 219–234.
  - 13 J. E. Burke, *Mol. Cell*, 2018, **71**, 653–673.
  - 14 T. E. J. Phillips and E. Maguire, *Front. Cell. Neurosci.*, 2021, **15**, 652593.
  - 15 A. Beziau, D. Brand and E. Piver, *Viruses*, 2020, **12**, 1124.
  - 16 M. D. Goncalves, B. D. Hopkins and L. C. Cantley, *N. Engl. J. Med.*, 2018, **379**, 2052–2062.
  - 17 G. K. Arora, L. Palamiuc and B. M. Emerling, *FEBS Lett.*, 2022, **596**, 3–16.
  - 18 Y. J. Shin, J. K. Sa, Y. Lee, D. Kim, N. Chang, H. J. Cho, M. Son, M. Y. T. Oh, K. Shin, J. K. Lee, J. Park, Y. K. Jo, M. Kim, P. J. Paddison, V. Tergaonkar, J. Lee and D. H. Nam, *J. Exp. Med.*, 2019, **216**, 1120–1134.
  - 19 J. Triscott, M. Reist, L. Küng, F. C. Moselle, M. Lehner, J. Gallon, A. Ravi, G. K. Arora, S. de Brot, M. Lundquist, H. Gallart-Ayala, J. Ivanisevic, S. Piscuoglio, L. C. Cantley, B. M. Emerling and M. A. Rubin, *Sci. Adv.*, 2023, **9**, eade8641.
  - 20 J. G. Jude, G. J. Spencer, X. Huang, T. D. D. Somerville, D. R. Jones, N. Divecha and T. C. P. Somerville, *Oncogene*, 2015, **34**, 1253–1262.
  - 21 S. Zhang, Z. Li, X. Yan, L. Bao, Y. Deng, F. Zeng, P. Wang, J. Zhu, D. Yin, F. Liao, X. Zhou, D. Zhang, X. Xia, H. Wang, X. Yang, W. Zhang, H. Gao, W. Zhang, L. Yang, Q. Hou, H. Xu, Y. Zhang, Y. Shu and Y. Wang, *Front. Genet.*, 2019, **9**, 721.
  - 22 B. M. Emerling, J. B. Hurov, G. Poulogiannis, K. S. Tsukazawa, R. Choo-Wing, G. M. Wulf, E. L. Bell, H. S. Shim, K. A. Lamia, L. E. Rameh, G. Bellinger, A. T. Sasaki, J. M. Asara, X. Yuan, A. Bullock, G. M. Denicola, J. Song, V. Brown, S. Signoretti and L. C. Cantley, *Cell*, 2013, **155**, 844–857.
  - 23 A. Ravi, L. Palamiuc, R. M. Loughran, J. Triscott, G. K. Arora, A. Kumar, V. Tieu, C. Pauli, M. Reist, R. J. Lew, S. L. Houlihan, C. Fellmann, C. Metallo, M. A. Rubin and B. M. Emerling, *Dev. Cell*, 2021, **56**, 1661–1676.e10.
  - 24 K. Lima, J. L. Coelho-Silva, G. S. Kinker, D. A. Pereira-Martins, F. Traina, P. A. C. M. Fernandes, R. P. Markus, A. R. Lucena-Araujo and J. A. Machado-Neto, *Cancer Genet.*, 2019, **233–234**, 56–66.
  - 25 K. Lima, D. A. Pereira-Martins, L. B. L. de Miranda, J. L. Coelho-Silva, G. da S. Leandro, I. Weinhäuser, R. de C. Cavaglieri, A. de M. Leal, W. F. da Silva, A. P. A. de L. Lange, E. D. R. P. Velloso, E. Griessinger, J. R. Hilberink, E. Ammatuna, G. Huls, J. J. Schuringa, E. M. Rego and J. A. Machado-Neto, *Blood Cancer J.*, 2022, **12**, 151.
  - 26 S. C. Sivakumaren, H. Shim, T. Zhang, F. M. Ferguson, M. R. Lundquist, C. M. Browne, H. S. Seo, M. N. Paddock, T. D. Manz, B. Jiang, M. F. Hao, P. Krishnan, D. G. Wang, T. J. Yang, N. P. Kwiatkowski, S. B. Ficarro, J. M. Cunningham, J. A. Marto, S. Dhe-Paganon, L. C. Cantley and N. S. Gray, *Cell Chem. Biol.*, 2020, **27**, 525–537.e6.
  - 27 M. Kitagawa, P. J. Liao, K. H. Lee, J. Wong, S. C. Shang, N. Minami, O. Sampetean, H. Saya, D. Lingyun, N. Prabhu, G. K. Diam, R. Sobota, A. Larsson, P. Nordlund, F. McCormick, S. Ghosh, D. M. Epstein, B. W. Dymock and S. H. Lee, *Nat. Commun.*, 2017, **8**, 2200.
  - 28 T. D. Manz, S. C. Sivakumaren, F. M. Ferguson, T. Zhang, A. Yasgar, H. S. Seo, S. B. Ficarro, J. D. Card, H. Shim, C. V. Miduturu, A. Simeonov, M. Shen, J. A. Marto, S. Dhe-Paganon, M. D. Hall, L. C. Cantley and N. S. Gray, *J. Med. Chem.*, 2020, **63**, 4880–4895.
  - 29 T. D. Manz, S. C. Sivakumaren, A. Yasgar, M. D. Hall, M. I. Davis, H. S. Seo, J. D. Card, S. B. Ficarro, H. Shim, J. A. Marto, S. Dhe-Paganon, A. T. Sasaki, M. B. Boxer, A. Simeonov, L. C. Cantley, M. Shen, T. Zhang, F. M. Ferguson and N. S. Gray, *ACS Med. Chem. Lett.*, 2020, **11**, 346–352.
  - 30 T. P. C. Rooney, G. G. Aldred, H. K. Boffey, H. M. G. Willems, S. Edwards, S. J. Chawner, D. E. Scott, C. Green, D. Winpenny, J. Skidmore, J. H. Clarke and S. P. Andrews, *J. Med. Chem.*, 2023, **66**, 804–821.
  - 31 L. Wortmann, N. Bräuer, S. J. Holton, H. Irlbacher, J. Weiske, C. Lechner, R. Meier, J. Karén, C. B. Siöberg, V. Pütter, C. D. Christ, A. Ter Laak, P. Lienau, R. Lesche, B. Nicke, S. H. Cheung, M. Bauser, A. Haegebarth, F. Von Nussbaum, D. Mumberg and C. Lemos, *J. Med. Chem.*, 2021, **64**, 15883–15911.
  - 32 D. H. Drewry, F. M. Potjewyd, J. L. Smith, S. Howell and A. D. Axtman, *Curr. Res. Chem. Biol.*, 2023, **3**, 100036.
  - 33 H. M. G. Willems, S. Edwards, H. K. Boffey, S. J. Chawner, C. Green, T. Romero, D. Winpenny, J. Skidmore, J. H. Clarke and S. P. Andrews, *RSC Med. Chem.*, 2023, **14**, 934–946.
  - 34 I. Al-Ramahi, S. S. P. Giridharan, Y.-C. Chen, S. Patnaik, N. Safren, J. Hasegawa, M. de Haro, A. K. W. Gee, S. A. Titus, H. Jeong, J. Clarke, D. Krainc, W. Zheng, R. F. Irvine, S. Barmada, M. Ferrer, N. Southall, L. S. Weisman, J. Botas and J. J. Marugan, *elife*, 2017, **6**, e29123.
  - 35 S. Chen, C. C. Tjin, X. Gao, Y. Xue, H. Jiao, R. Zhang, M. Wu, Z. He, J. Ellman and Y. Ha, *Proc. Natl. Acad. Sci. U. S. A.*, 2021, **118**, e2002486118.



- 36 W. Ji, E. S. Wang, T. D. Manz, J. Jiang, K. A. Donovan, X. Abulaiti, E. S. Fischer, L. C. Cantley, T. Zhang and N. S. Gray, *Eur. J. Med. Chem.*, 2023, **247**, 115027.
- 37 Note that, as previously reported in ref. 30 and 38 a “PI5P4K $\gamma$ ” ADP-Glo assay is used for routine screening and a PI5P4K $\gamma$  wild-type InCELL Pulse assay is later used to verify PI5P4K $\gamma$  activity with series exemplars.
- 38 H. K. Boffey, T. P. C. Rooney, H. M. G. Willems, S. Edwards, C. Green, T. Howard, D. Ogg, T. Romero, D. E. Scott, D. Winpenny, J. Duce, J. Skidmore, J. H. Clarke and S. P. Andrews, *J. Med. Chem.*, 2022, **65**, 3359–3370.

